nature chemical biology

Article

https://doi.org/10.1038/s41589-022-01220-2

Structural basis for heparan sulfate co-polymerase action by the EXT1–2 complex

In the format provided by the authors and unedited

Supplementary Information for

Structural basis for heparan sulfate co-polymerase action by the EXT1-2 complex

Hua Li, Digantkumar Chapla, Robert A. Amos, Annapoorani Ramiah,
Kelley W. Moremen, and Huilin Li

Supplementary Table 1: Cryo-EM data collection, refinement and validation statistics

	EXT1-2* (EMDB-25035) (PDB 7SCH)	UDP-GlcA* (EMDB-26702) (PDB 7UQY)	UDP-GlcNAc* (EMDB-26701) (PDB 7UQX)	4-mer complex* (EMDB-25036) (PDB 7SCJ)	7-mer complex* (EMDB-25037) (PDB 7SCK)
Data collection and processing					
Magnification	105,000	105,000	105,000	105,000	105,000
Voltage (kV)	300	300	300	300	300
Electron exposure ($e^-/Å^2$)	66.8	62	62	60	68/72
Defocus range (μm)	1.0-2.2	1.0-2.1	1.0-2.1	1.0-2.2	0.9-1.8
Pixel size (Å)	0.828	0.828	0.828	0.828	0.828
Symmetry imposed	C1	C1	C1	C1	C1
Initial particle images (No.)	5,186,047	4,871,613	4,783,612	1,938,290	5,509,005 +5,668,467
Final particle images (No.)	120,216	335,313	161,338	451,367	321,316
Map resolution (Å)	3.1	3.0	3.3	3.0	2.8
FSC threshold	0.143	0.143	0.143	0.143	0.143
Map resolution range (Å)	3.0-4.5	2.9-4.5	3.0-5.0	2.7-4.5	2.7-4.3
Refinement					
Initial model used (PDB code)	N/A	7SCH	7SCH	7SCH	7SCH
Model resolution (Å)	3.4	3.4	3.5	3.4	3.3
FSC threshold	0.5	0.5	0.5	0.5	0.5
Model resolution range (Å)	3.0-4.5	2.9-4.5	3.0-5.0	2.7-4.5	2.8-4.5
Map sharpening *B* factor ($Å^2$)	88.7	97.0	93.2	96.0	55.9
Model composition					
Non-hydrogen atoms	9,711	9,556	9,491	9,336	10,250
Protein residues	1,190	1,167	1,154	1,131	1,240
Ligands	3	4	7	9	11
B factors ($Å^2$)					
Protein	36.3	35.8	71.6	54.6	61.7
Ligand	27.4	24.5	72.7	48.6	44.7
R.m.s. deviations					
Bond lengths (Å)	0.003	0.003	0.002	0.004	0.004
Bond angles (°)	0.590	0.571	0.503	0.556	0.548
Validation					
Molprobity score	1.77	1.85	1.70	1.88	1.88
Clashscore	9.19	9.88	9.21	9.38	9.55
Poor rotamers (%)	0		0.29	0	0.36
Ramachandran plot					
Favored (%)	95.91	95.13	96.66	94.34	94.54
Allowed (%)	4.09	4.87	3.34	5.66	5.46
Disallowed (%)	0	0	0	0	0

*For the EXT1-2, UDP-GlcA, UDP-GlcNAc, 4-mer complex, and 7-mer complex dataset, a typical raw micrograph was provided in Supplementary Figure 1a, 3a, 4a, 6a, 7b, respectively.

Supplementary Table 2: Kinetic parameters for wild type EXT1-2 using oligosaccharide substrates (4-mer, 5-mer, 6-mer, 7-mer) and their respective donors in assays performed at 37°C for 1 h.

Acceptor substrates	Donors	K_m *(μM)*	k_{cat} *(min^{-1})*	k_{cat}/K_m *($min^{-1}mM^{-1}$)*
GlcNAc-GlcA-GlcNAc-GlcA-pNP (4-mer)	UDP-GlcA	602.6 ± 182.7	167.1 ± 25.82	277.4
GlcNAc-GlcA-GlcNAc-GlcA-GlcNAc-GlcA-pNP (6-mer)	UDP-GlcA	357.8 ± 98.65	42.58 ±6.35	119.3
GlcA-GlcNAc-GlcA-GlcNAc-GlcA-pNP (5-mer)	UDP-GlcNAc	56.48 ± 45.12	11.97 ± 3.494	213.7
GlcA-GlcNAc-GlcA-GlcNAc-GlcA-GlcNAc-GlcA-pNP (7-mer)	UDP-GlcNAc	235.2 ± 66.7	38.68 ± 5.043	164.6

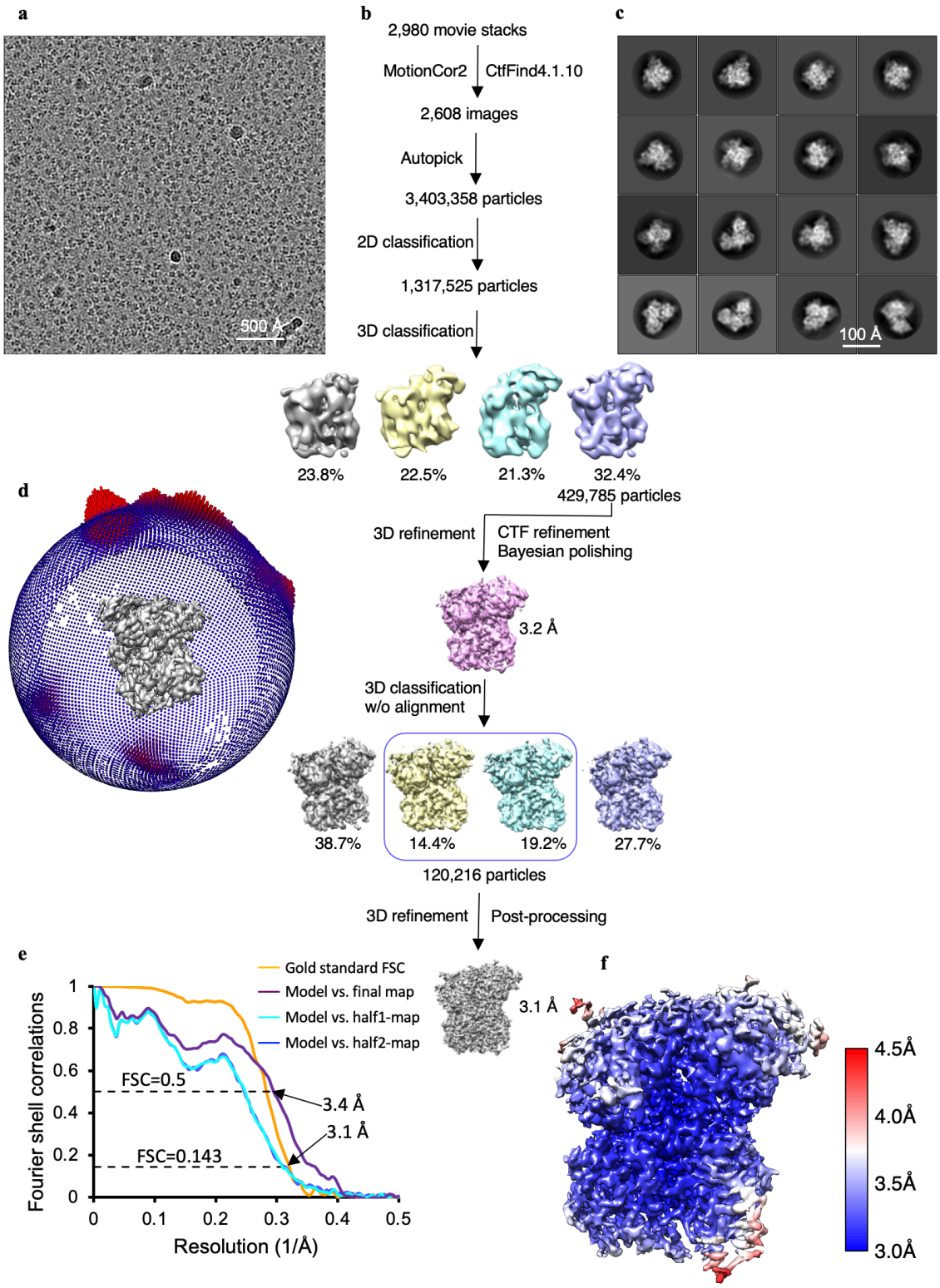

Supplementary Figure 1: Workflow for EXT1-2 cryo-EM structure determination. a, c, Representative micrograph from a total of 2,980 micrographs and selected 2D averages out of 32 class averages. **b**, Workflow of cryo-EM data processing. **d**, Eulerian angle distribution of particles used for 3D reconstruction. **e**, Gold-standard Fourier shell correlations. f, Local resolution map.

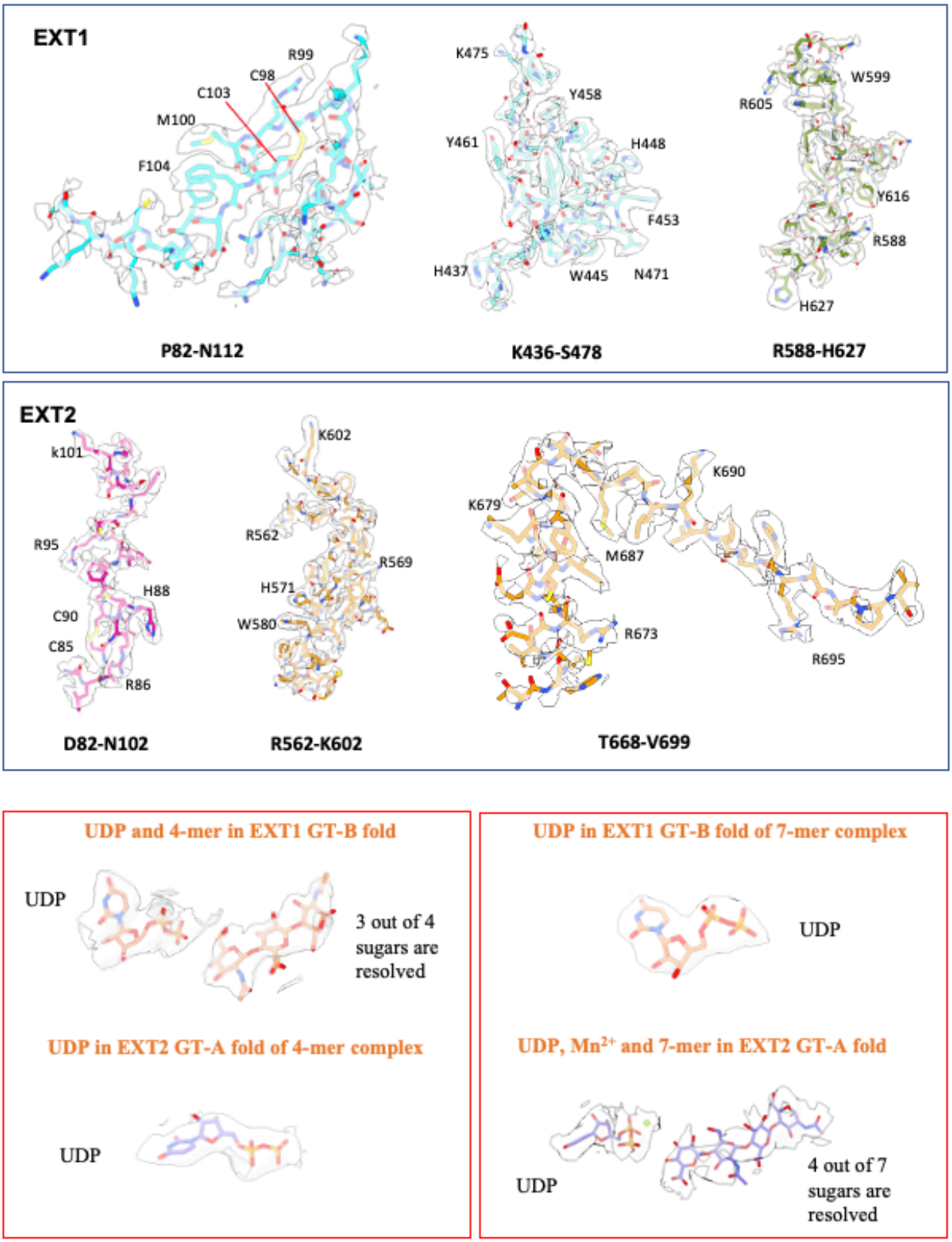

Supplementary Figure 2: Fitting of the atomic model with the EM map in several selected regions, including the bound ligand densities in the catalytic pockets.

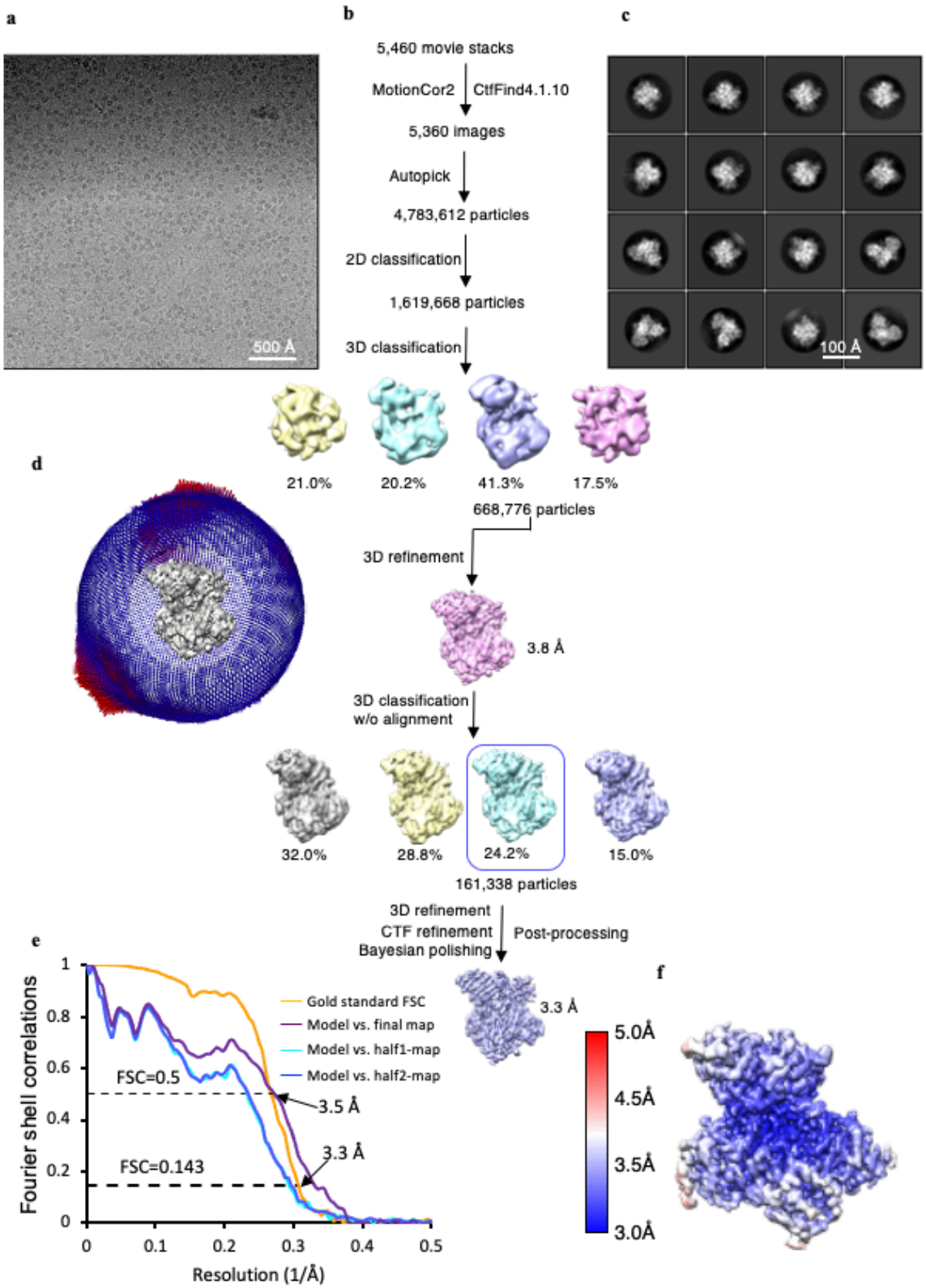

Supplementary Figure 3: Workflow for UDP-GlcNAc complex cryo-EM structure determination. a, c, Representative micrograph from a total of 5,460 micrographs and selected 2D averages out of 18 class averages. **b**, Workflow of cryo-EM data processing. **d**, Eulerian angle

distribution of particles used for 3D reconstruction. **e**, Gold-standard Fourier shell correlations. **f**, Local resolution map.

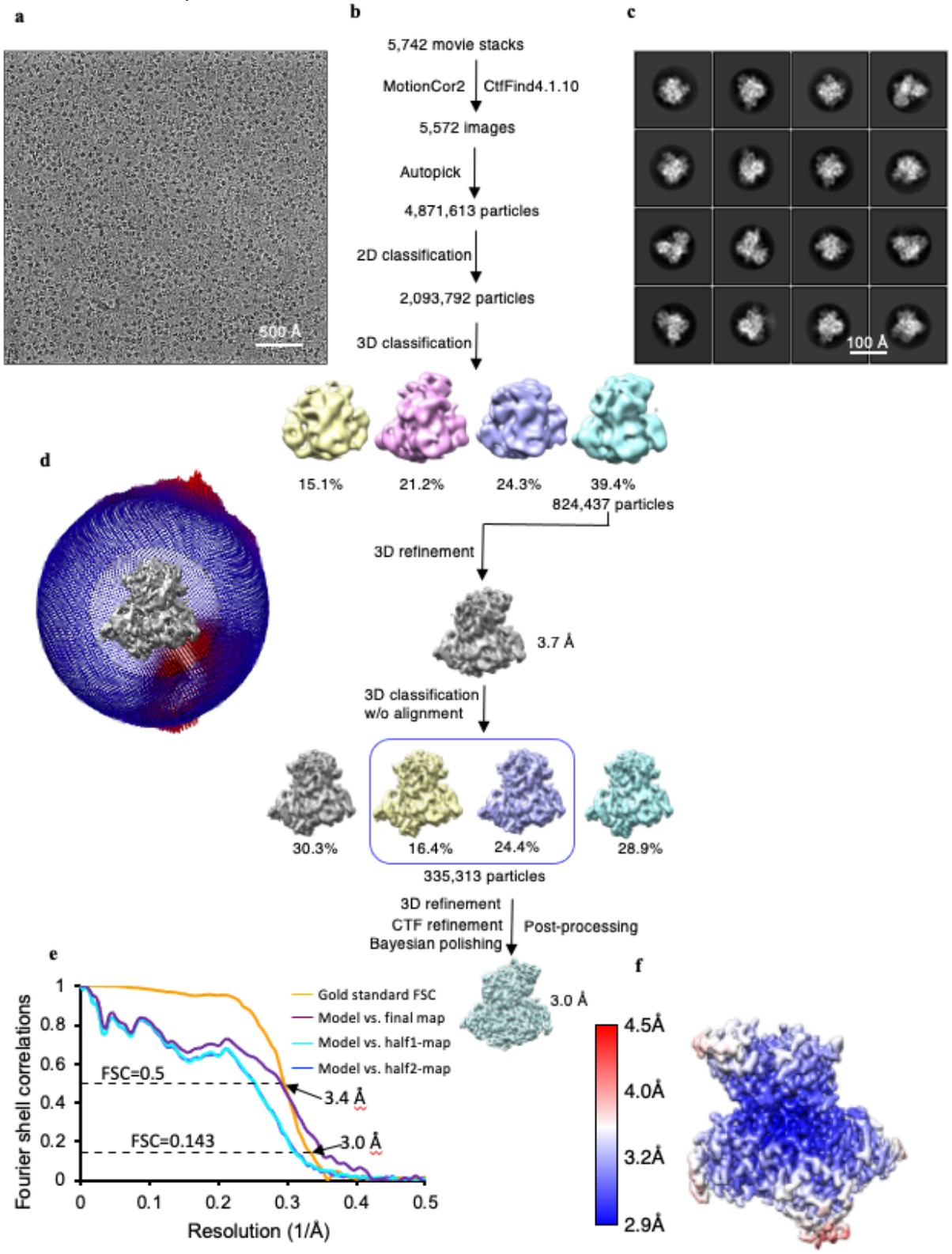

Supplementary Figure 4: Workflow for UDP-GlcA complex cryo-EM structure determination. a, c, Representative micrograph from a total of 5,742 micrographs and selected

2D averages out of 26 class averages. **b**, Workflow of cryo-EM data processing. **d**, Eulerian angle distribution of particles used for 3D reconstruction. e, Gold-standard Fourier shell correlations. **f**, Local resolution map.

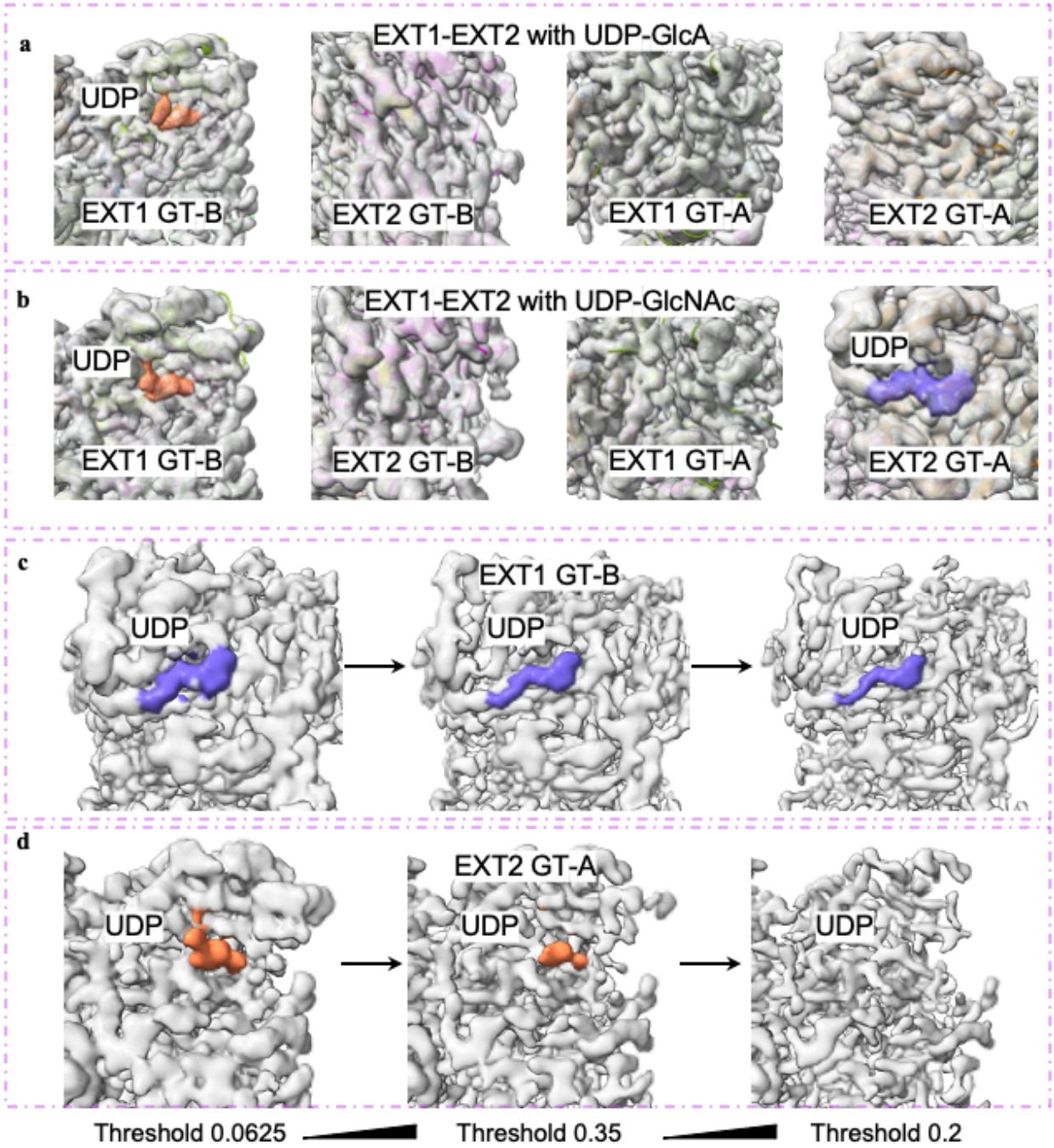

Supplementary Figure 5: EM densities in the catalytic pockets of EXT1 and EXT2 shown with increasing display threshold. a, close-up view of EXT1 GT-B cleft, EXT2 GT-B cleft, EXT1 GT-A cleft, and EXT2 GT-A cleft of 3D map of EXT1-2 complexed with UDP-GlcA. **b**, close-up view of EXT1 GT-B cleft, EXT2 GT-B cleft, EXT1 GT-A cleft, and EXT2 GT-A cleft of 3D map of EXT1-2 complexed with UDP-GlcNAc. Close-up view of EXT2 GT-A cleft (**c**) and EXT1 GT-B cleft (**d**) in EXT1-2 complexed with UDP-GlcNAc at three different thresholds. Model was colored the

same as in Fig. 1. 3D map in light gray with the extra density at EXT1 GT-B cleft and EXT2 GT-A cleft in coral and slate blue, respectively.

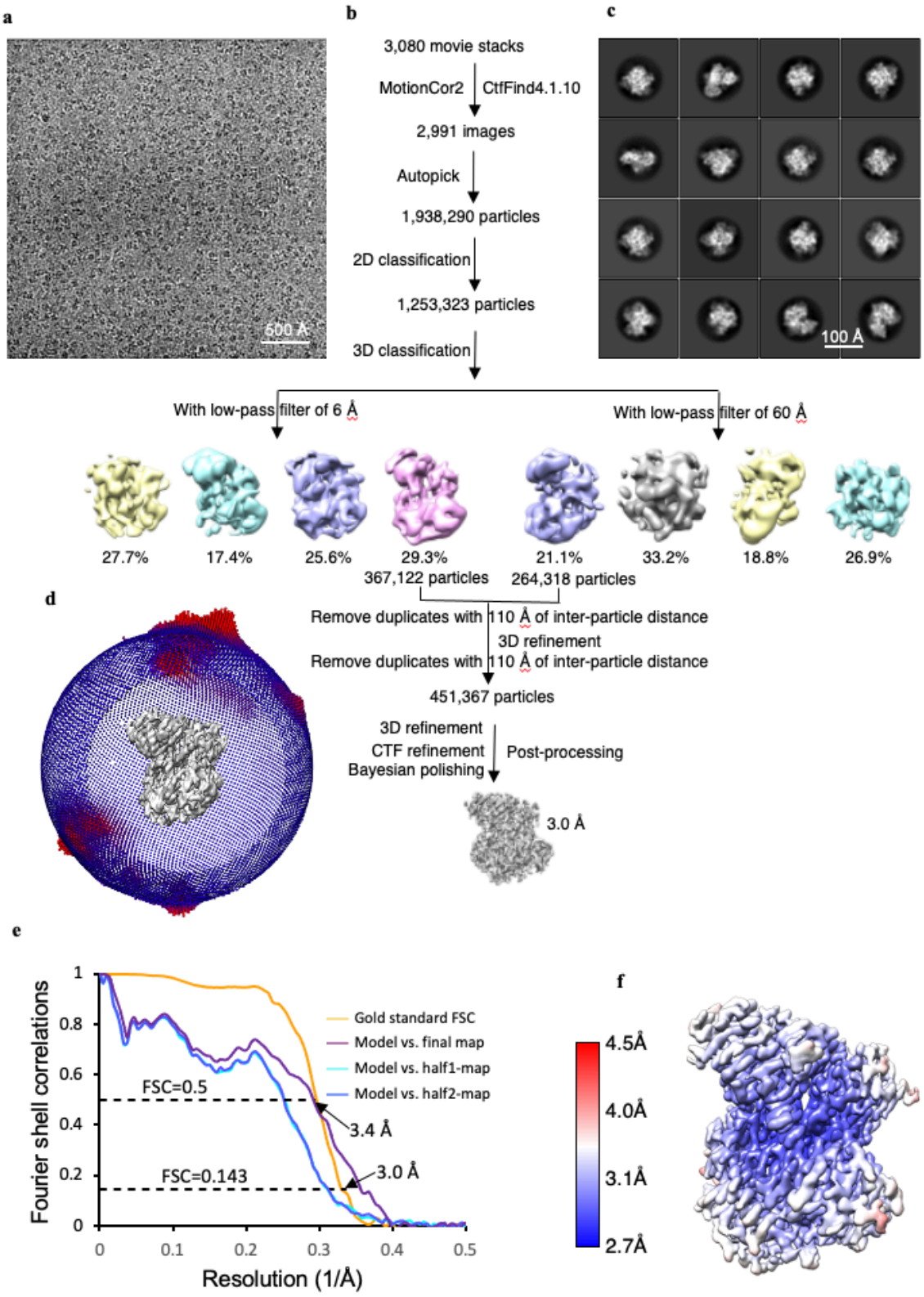

Supplementary Figure 6: Workflow for 4-mer complex cryo-EM structure determination. a, **c**, Representative micrograph from a total of 3,080 micrographs and selected 2D averages out of 37 class averages. **b**, Workflow of cryo-EM data processing. **d**, Eulerian angle distribution of

particles used for 3D reconstruction. **e**, Gold-standard Fourier shell correlations. **f**, Local resolution map.

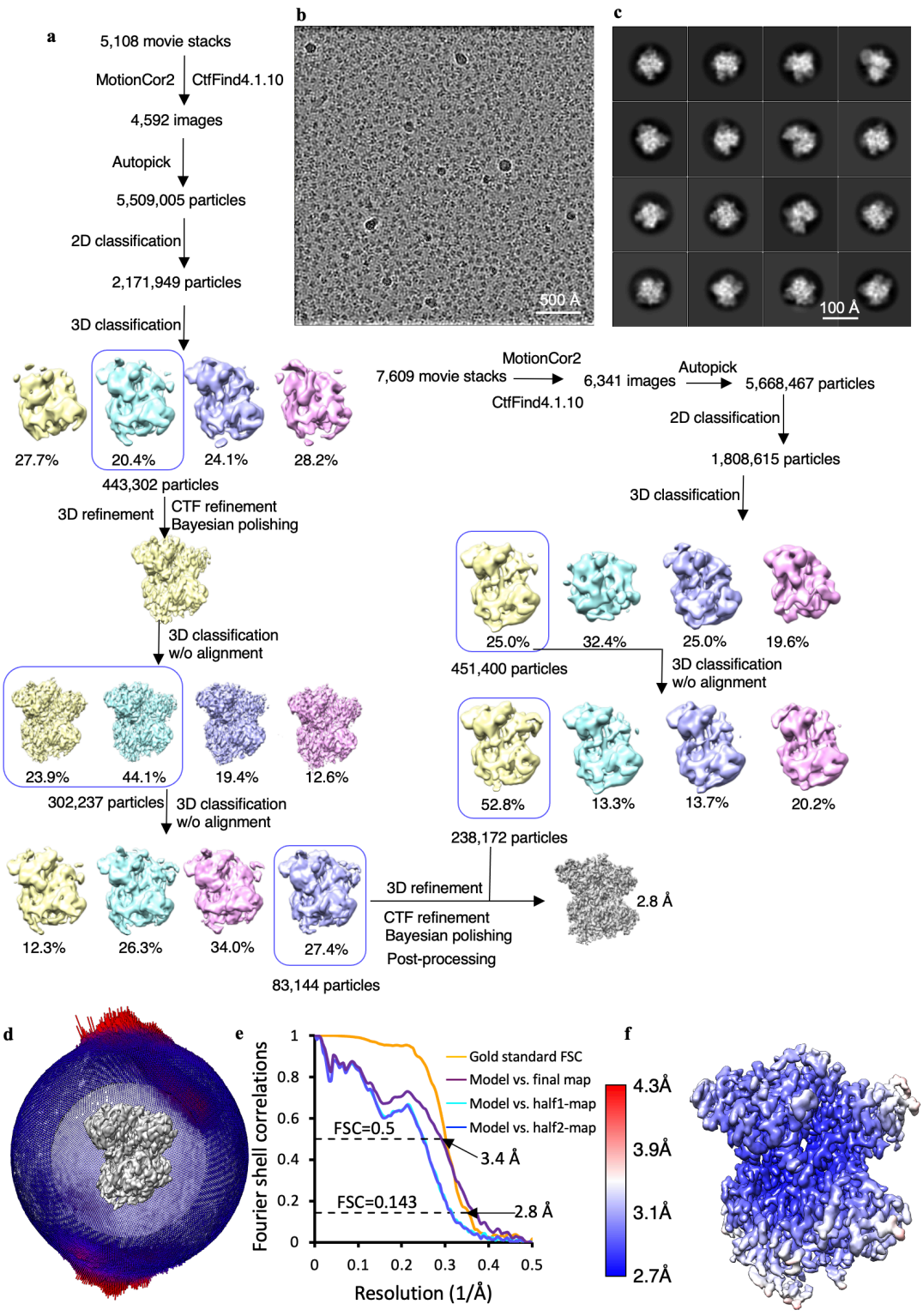

Supplementary Figure 7: Workflow for 7-mer complex cryo-EM structure determination. a, Workflow of cryo-EM data processing. **b, c**, Representative micrograph from a total of 12,717 micrographs and selected 2D averages out of 38 class averages. **d**, Eulerian angle distribution of particles used for 3D reconstruction. **e**, Gold-standard Fourier shell correlations. **f**, Local resolution map.